

pubs.acs.org/JPCA Article

# Spectroscopic Characterization of the Divalent Metal Docking Motif to Isolated Cyanobenzoate: Direct Observation of Tridentate Binding to *ortho*-Cyanobenzoate and Implications for the CN Response

Published as part of The Journal of Physical Chemistry A virtual special issue "Honoring Michael R. Berman". Ahmed Mohamed, Sean C. Edington, Maxim Secor, James R. Breton, Sharon Hammes-Schiffer, and Mark A. Johnson\*



Cite This: J. Phys. Chem. A 2023, 127, 1413-1421



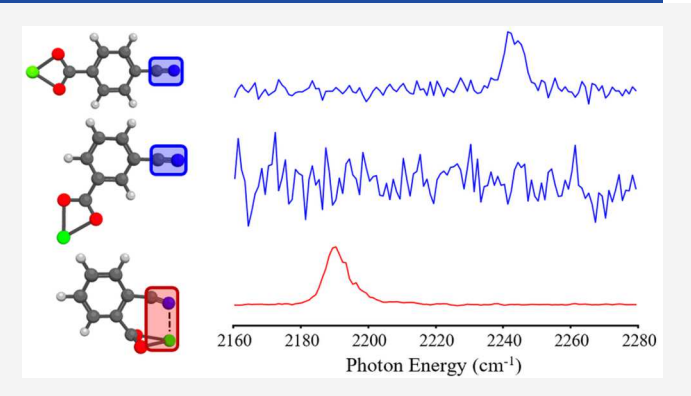
**ACCESS** 

Metrics & More

Article Recommendations

s Supporting Information

**ABSTRACT:** Cryogenic ion vibrational spectra of  $D_2$ -tagged cyanobenzoate (CBA) derivatives are obtained and analyzed to characterize the intrinsic spectroscopic responses of the  $-CO_2^-$  headgroup to its location on the ring in both the isolated anions and the cationic complexes with divalent metal ions,  $M^{2+}$  (M=Mg, Ca, Sr). The benzonitrile functionality establishes the different ring isomers (*para, meta, ortho*) according to the location of the carboxylate and provides an additional reporter on the molecular response to the proximal charge center. The aromatic carboxylates display shifts slightly smaller than those observed for a related aliphatic system upon metal ion complexation. Although the CBA anions display very similar band patterns for all three ring positions, upon complexation with metal ions, the *ortho* isomer



yields dramatically different spectral responses in both the  $-CO_2^-$  moiety and the CN group. This behavior is traced to the emergence of a tridentate binding motif unique to the *ortho* isomer in which the metal ions bind to both the oxygen atoms of the carboxylate group and the N atom of the cyano group. In that configuration, the  $-CO_2^-$  moiety is oriented perpendicular to the phenyl ring, and the CN stretching fundamental is both strong and red-shifted relative to its behavior in the isolated neutral. The behaviors of the metal-bound *ortho* complexes occur in contrast to the usual blue shifts associated with "Lewis" type binding of metal ions end-on to -CN. The origins of these spectroscopic features are analyzed with the aid of electronic structure calculations, which also explore differences expected for complexation of monovalent cations to the *ortho* carboxylate. The resulting insights have implications for understanding the balance between electrostatic and steric interactions at metal binding sites in chemical and biological systems.

# I. INTRODUCTION

In isolation, divalent metal ions typically bind to the carboxylate anionic headgroup of a molecule in a bidentate fashion with respect to the oxygen atoms. This structural motif is indirectly encoded in the behavior of the CO stretching fundamentals of the carboxylate group, and using this diagnostic, the bidentate binding mode is found in biological ionophores. The influence of the local solvation environment on these spectroscopic signatures has been explored in microhydrated metal ion complexes with aliphatic R-CO<sub>2</sub> anions using cryogenic ion vibrational spectroscopy. Here we extend that work to include the cyanobenzoate isomers depicted in Figure 1, which introduce the new feature that the carboxylate group participates in the aromaticity associated with sp<sup>2</sup> carbon atoms in the ring. This intramolecular

interaction is evidenced by the fact that the isolated benzoate anion is planar, which can be rationalized by partial charge delocalization onto the ring. Quantifying the spectroscopic behaviors of the benzoates thus explores the question of how partial delocalization of the excess charge affects the response of the CO stretching bands both as isolated anions and in the cationic complexes formed by attachment of divalent metal ions,  $M^{2+}$  (M = Ca, Mg, Sr) onto the carboxylate group.

Received: October 31, 2022 Revised: December 21, 2022 Published: February 7, 2023





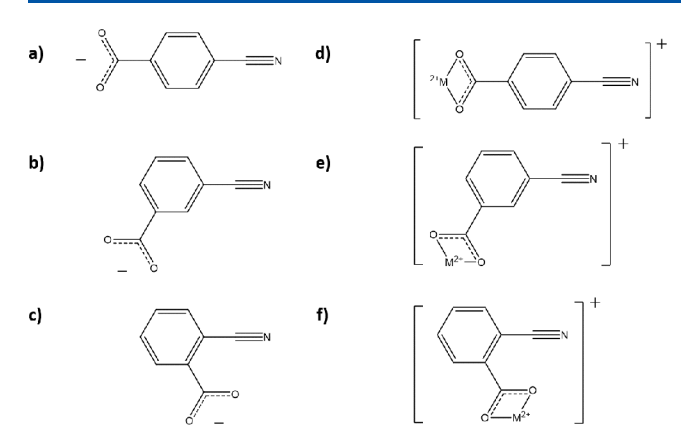


**Figure 1.** Schematic of the three cyanobenzoate isomers (a,b,c) corresponding to 4-, 3-, and 2-CBA, respectively, and the metal complexes (d,e,f) explored in this study.

Further, to determine how the  $CO_2^-$  and  $CO_2^-/M^{2+}$  charge centers affect substituents bound to the ring, we exploit the fact that the CN group is widely used to monitor electric field effects in complex condensed media 7-9 such as enzyme active sites.<sup>7,10–12</sup> It is of particular interest to elucidate how metal binding occurs in the ortho-cyanobenzoate in which the charge center resides closest to the cyano group. This aspect of the study thus establishes how the CN fundamental responds to proximal charges in the absence of competing effects (e.g., electric field, hydrogen bonding, molecular conformation) that contribute to the spectroscopic readout 8,13,14 in the condensed phase. We establish the structures adopted by these molecular anions and their metal complexes by analyzing their vibrational band patterns obtained by cryogenic vibrational spectroscopy of the He- and D2-tagged, mass-selected ions. This structural information, in turn, provides a well-defined platform for unraveling the factors driving the spectral response of the CN group.

#### **IIA. EXPERIMENTAL METHODS**

Infrared predissociation (IRPD) spectra of isolated molecules cooled to ~20 K were collected using the Yale hybrid photofragmentation mass spectrometer ("Yale spectrometer"), which has been described previously. 15 Briefly, the instrument couples a ThermoFisher Scientific Orbitrap Velos Pro mass spectrometer (hereafter "Velos") with a custom-built, triplefocusing tandem time-of-flight ("TOF") mass spectrometer. The Velos was used to survey different solution preparations for stable electrospray ionization ("ESI") prior to collection of IRPD spectra. In a typical experiment, ions produced using the Velos ESI source were transferred to the Yale custom-built spectrometer for infrared spectroscopy. Following extraction from solution via ESI using the Velos ion source, the molecules under study ("ions") are isolated in high vacuum ( $\sim 10^{-6}$  Torr) through multiple differential pumping stages and held in a radio frequency Paul trap. The ions are decelerated and cooled in the Paul trap via collisions with pulsed He buffer gas. The buffer gas is doped with a "mass tag," typically H2 or D2, which weakly attaches to the ions at low temperature (10-30 K). For ions with sufficiently exposed charge centers, minimally perturbative tagging with He is utilized. Following cooling and attachment, the tagged ions are extracted into the TOF stage of the instrument in a Wiley-McLaren configuration. The ions, thus mass-selected, are intersected with a midinfrared laser pulse ( $\sim 10$  ns,  $\sim 1$  mJ, 800-4000 cm<sup>-1</sup>)

produced by an OPO/OPA system (LaserVision) with a subsequent conversion to the 5–10  $\mu$ m range in AgGaSe<sub>2</sub>. When the laser pulse is resonant with a vibrational mode of a given molecular ion, the weakly bound mass tag is dissociated via intramolecular vibrational redistribution, allowing collection of the linear, single-photon infrared action spectrum that can be directly compared to predictions produced using electronic structure calculations. para-, meta-, and ortho-Cyanobenzoic acid (hereafter: 4-CBA, 3-CBA, and 2-CBA, respectively) were purchased from Sigma-Aldrich and used as received. Mg(NO<sub>3</sub>)<sub>2</sub>, Ca(NO<sub>3</sub>)<sub>2</sub>, and Sr(NO<sub>3</sub>)<sub>2</sub> were purchased from Sigma-Aldrich and used as received. Solutions 1 mM in 2-, 3, or 4-CBA acid and 1 mM of a given metal nitrate were prepared by sonication in 1:1 (v:v) methanol:water until the mixture was clear. Solutions were directly introduced into the Velos or Yale spectrometer via ESI.

#### **IIB. THEORETICAL METHODS**

Geometry optimizations and frequency calculations were performed on all cyanobenzoate species using second-order Møller–Plesset perturbation theory 16–18 (MP2). Similar results were obtained with density functional theory (DFT) using the B3LYP-D3 functional. The 6-311++G(d,p) atomic basis set 19–22 was used for all electronic structure calculations in this study. Relaxed scans were conducted about the dihedral angle between the cyanobenzoate rings and carboxylate groups using MP2. All MP2 and DFT calculations reported in this paper were performed using the Gaussian16 electronic structure program. Additional computational details are provided in the Supporting Information, section S1.

The full infrared spectra were computed within the harmonic approximation by diagonalization of the mass-weighted Hessian at optimized geometries to produce the normal modes. For calculated results reported in the figures and tables, spectra were scaled by 0.975 below 2000 cm<sup>-1</sup> to match the carboxylate peaks. Spectra were scaled by 1.029 above 2000 cm<sup>-1</sup> for comparison with measured frequencies for nitrile stretching transitions. This calibration factor gives agreement between experiment and the same level of computation for the nitrile stretch in neutral benzonitrile.

#### III. RESULTS AND DISCUSSION

Figure 2 panels b-d present the D<sub>2</sub>-tagged IRPD spectra of the three cyanobenzoates indicated in the insets, along with that previously reported<sup>2</sup> for the propionate (CD<sub>3</sub>CD<sub>2</sub>CO<sub>2</sub><sup>-</sup>, hereafter d-OPr<sup>-</sup>) anion in Figure 2a. The latter isotopologue was chosen to suppress activity arising from the CH bending modes in the region of the CO stretches. All four spectra are dominated by the strong CO<sub>2</sub> modes arising from the symmetric stretch ( $u_{\rm s}^{\rm CO}$ ) near 1320 cm $^{-1}$  and the asymmetric stretch  $(\nu_{as}^{CO})$  near 1650 cm<sup>-1</sup>, with the observed trends collected in Table 1. We note that although this notation is often used, the normal mode displacement vectors associated with the "symmetric stretch" transition actually involves a significant contribution from the C-C bond between the carbon atoms that attach the headgroup to the ring. The asymmetric stretch is more localized on the  $-\mathrm{CO}_2^-$  moiety, and at a qualitative level, the  $u_{\rm as}^{\rm CO}$  band position reflects the electron density on the headgroup. Specifically, increased electron density on the  $-CO_2^-$  moiety leads to increased population of the CO antibonding orbitals.<sup>5,24</sup> This is manifest in elongation of the CO bond lengths and concomitant red

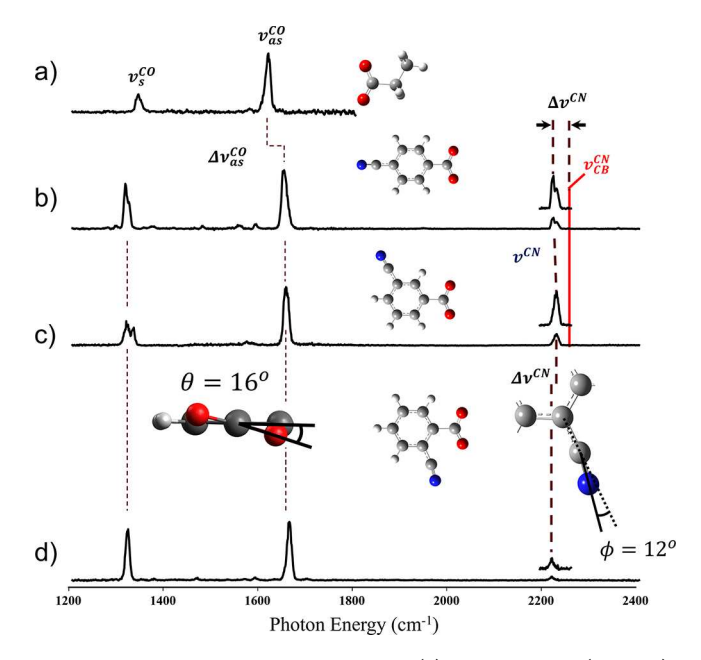


Figure 2. D<sub>2</sub>-tagged IRPD spectra of the (a) propionate- $d_5$  (d-OPr<sup>-</sup>), (b) 4-cyanobenzoate (4-CBA<sup>-</sup>), (c) 3-CBA<sup>-</sup>, and (d) 2-CBA<sup>-</sup> anions. Structures of the cyanobenzoates predicted at the MP2/6-311++G(d,p) level of theory are displayed as insets, with expanded regions of the 2-CBA<sup>-</sup> structure indicated in (d) to highlight intramolecular distortions. Spectral insets near 2200 cm<sup>-1</sup> display 3× expansions of the CN stretch fundamentals. The symmetric carboxylate stretch, asymmetric carboxylate stretch, and nitrile stretch are denoted by  $\nu_{\rm s}^{\rm CO}$ ,  $\nu_{\rm as}^{\rm CO}$ , and  $\nu_{\rm s}^{\rm CN}$ , respectively.

shift in the  $\nu_{\rm as}^{\rm CO}$  band. In this context, the main difference in the CO band response of the aliphatic system compared to the benzoates (Figure 2a) is that, for the former, the two bands are slightly closer together. The largest difference is a ~30 cm<sup>-1</sup> blue shift in the CO asymmetric stretch, which is consistent with the expectation that the CBA anions feature a small amount of electron delocalization on the ring. The blue shift is observed to increase by 5 and 7 cm<sup>-1</sup>, respectively, in going from 4-CBA to 3-CBA and finally to 2-CBA, illustrating the magnitude of the role played by the interaction with the proximal -CN group. These empirical observations and

assignments are recovered by electronic structure calculations with comparisons presented in Figure S1.

We next turn to the weaker CN stretch fundamental near 2220 cm<sup>-1</sup>. This band is evident in the spectra of all three CBA isomers, but its intensity decreases significantly (by about a factor of 3) going from 3- to 2-CBA. On the other hand, the changes in the frequencies for the three isomers (see values in Table 1) are within 10 cm $^{-1}$ , with the band in 4-CBA appearing as a closely space doublet. They all fall significantly (~20 cm<sup>-1</sup>) below the band in isolated cyanobenzene<sup>25</sup> (2242 cm<sup>-1</sup>, indicated by the red arrow  $(\Delta \nu_{\rm CB}^{\rm CN})$  in Figure 2b). From the structural standpoint, the most significant difference occurs in the calculated behavior of the 2-CBA anion. Its minimum energy structure is displayed in Figure 2d, illustrating that the carboxylate functionality directly interacts with the CN group. This is clearly a repulsive interaction between one of the -CO<sub>2</sub> oxygen atoms and the N atom of the nitrile group, with the distortions highlighted in the expanded inserts flanking the overall structure in Figure 2d. The CN group is displaced about 12° away from the symmetry axis of the ring position ( $\phi$  in Figure 2d), while the carboxylate group is rotated by  $\sim 16^{\circ}$  ( $\theta$  in Figure 2d) out of the plane of the ring. Values of key parameters associated with the calculated minimum energy structures are collected in Table 2.

To further explore the intramolecular interactions in play in the CBA anions, Figure 3 compares the calculated potential energy for rotation of the  $-CO_2^-$  group about the C-C axis that binds it to the ring, constraining  $\theta$  while allowing all other degrees of freedom to relax, for all three isomers. The curves are offset so that all the minima are placed at a common energy. The barriers relative to the minimum energy configuration are predicted to be about the same for 4- and 3-CBA but reduced by about 40% (from 3.92 to 2.48 kcal/mol for para to ortho) for the ortho isomer compared to those of the other two isomers. This quantifies the large magnitude of the repulsive interaction when the two groups are closest in the ortho species. In this case, the barrier is lowered because the repulsive interaction substantially raises the energy of the planar configuration, and this effect is reduced when the carboxylate is oriented perpendicular to the ring. A comparison of the absolute energies of the three isomers along the carboxylate rotation angle is presented in Figure S2.

Table 1. Experimental (±5 cm<sup>-1</sup>) Bands (Bold), Scaled Harmonic Frequencies (in Parentheses), Mode Character Assignments, and Nitrile Transition Intensities for the Ions and Metal Complexes Considered by This Work<sup>a</sup>

species	$ u_{\rm s}^{\rm CO}~({\rm cm}^{-1})$	$ u_{\rm as}^{\rm CO}~({\rm cm}^{-1})$	$ u^{\alpha} \left( \mathrm{cm}^{-1} \right)$	$ u^{eta}\ (\mathrm{cm}^{-1})$	$ u^{\mathrm{CN}}\ (\mathrm{cm}^{-1})$	$I^{\mathrm{CN}}$ (unitless)
d-OPr <sup>-</sup>	1344 (1367)	<b>1620</b> (1642)				
[Ca d-OPr]+	<b>1461</b> (1468)	1431 (1443)				
4-CBA	1313 (1333)	<b>1648</b> (1667)			<b>2216, 2225</b> (2229)	<b>0.19</b> (0.079)
3-CBA	<b>1316, 1329</b> (1302)	1653 (1674)			<b>2225</b> (2233)	0.20 (0.046)
2-CBA	1317 (1298)	<b>1660</b> (1674)			<b>2215</b> (2217)	0.063 (0.011)
[Mg 4-CBA] <sup>+</sup>	<b>1385, 1434</b> (1361, 141	1, 1426)	<b>1503</b> (1508)	<b>1603</b> (1607)	2242 (2230)	0.022 (0.021)
[Ca 4-CBA]+	<b>1393, 1431</b> (1367, 142	8, 1436)	<b>1501</b> (1507)	<b>1606</b> (1607)	<b>2243</b> (2231)	0.0053 (0.010)
[Ca 3-CBA] <sup>+</sup>	<b>1389, 1411, 1425, 145</b> (1393, 1412, 1435, 146		<b>1582</b> (1589)	<b>1604</b> (1607)	N.R. (2246)	<b>N.R.</b> (0.017)
[Ca 2-CBA] <sup>+</sup>	1415 (1412)	<b>1486</b> (1511)			<b>2190</b> (2219)	0.33 (0.33)
[Sr 2-CBA] <sup>+</sup>	1425	1511			2202	0.30

<sup>a</sup>Labels:  $\nu_{\rm s}^{\rm CO}$ , carboxylate symmetric stretch;  $\nu_{\rm as}^{\rm CO}$ , carboxylate asymmetric stretch;  $\nu^{\rm a}$  and  $\nu^{\rm b}$ , mixed modes involving dominant CH displacement;  $\nu^{\rm CN}$ , nitrile stretch; and  $I^{\rm CN}$ , intensity of the nitrile stretch expressed as a fraction of the strongest transition in the spectrum, which in all cases contains  $\nu_{\rm s}^{\rm CO}$  character. Due to mixing between the carboxylate stretching modes, C–C stretching modes, and CH modes in the metal complexes with 3- and 4-CBA, transitions containing these mixed characters are grouped together under the  $\nu_{\rm s}^{\rm CO}$  and  $\nu_{\rm as}^{\rm CO}$  labels for these species. See Section IIB for discussion of computational scaling factors.

Table 2. Calculated (MP2/6-311++G(d,p)) Structural Parameters for the Ions and Metal Complexes Considered by This Work<sup>a</sup>

species	$R_{\rm CO}$ (Å)	∠COO (deg)	$\omega_{ ext{COO}}  ext{ (deg)}$	$\omega_{ m COO}$ barrier height (kcal/mol)	$R_{\rm N-M}$ (Å)	∠CCN (deg)
d-OPr <sup>-</sup>	1.25	129	N/A	N/A	N/A	N/A
d-[Ca OPr]+	1.27	118	N/A	N/A	N/A	N/A
4-CBA	1.26	131	2.20	3.92	N/A	0.07
3-CBA <sup>-</sup>	1.25	131	0.63	3.77	N/A	0.81
2-CBA	1.25	131	16.28	2.48	N/A	11.7
[Mg 4-CBA] <sup>+</sup>	1.30	118	1.74	9.79	9.14	0.01
[Ca 4-CBA] <sup>+</sup>	1.29	119	2.25	8.70	9.42	0.05
[Ca 3-CBA] <sup>+</sup>	1.29	119	1.82	7.79	8.16	0.63
[Ca 2-CBA] <sup>+</sup>	1.27	121	82.67	9.26	2.44	13.9
[K 2-CBA]	1.26	127	85.57	2.50	2.91	5.83

"Labels:  $R_{\rm CO}$  is the distance between an oxygen and the carbon atom in the carboxylate headgroup.  $\angle$ COO is the angle formed by the carboxylate headgroup.  $\omega_{\rm COO}$  is the dihedral angle between the plane of the benzene ring and the  $-{\rm CO}_2^-$  moiety. The  $\omega_{\rm COO}$  barrier height is the energy difference between the calculated minimum energy structure and the maximum energy as  $\omega_{\rm COO}$  is scanned (see Figures S2 and S3 for plots).  $R_{\rm N-M}$  is the distance from the nitrogen atom belonging to the nitrile group to the metal where applicable.  $\angle$ CCN is the angle formed by the nitrile and the aromatic carbon atom to which it is bound. See Table S2 and Table S3 for structural parameters from B3LYP calculations and for calculated Mulliken charges, respectively.

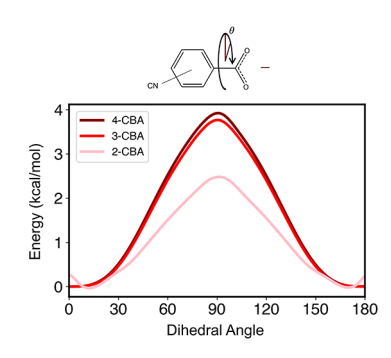


Figure 3. Calculated (MP2/6-311++G(d,p)) potential energy curves for rotation of the  $-\mathrm{CO_2}^-$  group about the C–C bond to the ring while relaxing all other degrees of freedom, where  $\theta=0$  corresponds to the planar structure. The curves are vertically offset so that each isomer's minimum occurs at 0. See Figure S2 for a comparison of absolute energies. See Figure S4 for analogous potential energy curves obtained using DFT.

The frequency of the CN stretch is red-shifted going from 3-CBA to 2-CBA, but it is not necessarily a reflection of structural distortion since the 2-CBA frequency is actually very close to the lower member of the doublet displayed by 4-CBA (see values in Table 1). The origin of this doublet is not presently known and is not accounted for at the harmonic level. The major effect of the structural distortions at play in 2-CBA on the vibrational spectrum is therefore the reduction in the intensity of the transition. This insensitivity of the CN frequency to the location of the negative charge center is curious given the fact that many recent reports have exploited its frequency shifts and intensity modulations as so-called "reporters" for the local electric fields in complex media. 7-11,26-28 The CBA isomers thus extend related studies that have considered how the nitrile H-bond-accepting environment affects the spectral shift. 13,14,29 We note that the intensity trends in the response of the CN reporter have been considered in the recent paper by Weaver et al., and that not only the presence but also the geometry of H-bonding partners plays a crucial role in the nitrile spectroscopic response. <sup>12–14,29</sup> In the spectra shown in Figure 2, the CN frequency is mainly reporting on the additional electronic

charge that delocalizes from the  $-CO_2^-$  group onto the ring, which appears to be similar for all three isomers.

IIIB. Vibrational Spectra of the M2+ Complexes with 2-, 3-, and 4-CBA. IIIB.1. Comparison with Aliphatic Complexation in the 4-CBA Complexes with Mg<sup>2+</sup> and  $Ca^{2+}$ . In light of the relative insensitivity of the CN stretch frequency with respect to the anionic charge center, we next consider the case of complexation with divalent cations (in this case Ca2+, Mg2+, and Sr2+), which are known to bind in a bidentate manner with the carboxylate group. 5,6 In effect, this modification converts the location of the anionic charge center into a net charge of +1, which again migrates around the ring according to the carboxylate location in the three CBA isomers. We begin with the 4-CBA complexes with Ca<sup>2+</sup> and Mg<sup>2+</sup>, which feature the largest separation between the nitrile group and the charge center. The divalent metal ions interact very strongly with D2 molecules, and we therefore monitored the IRPD behavior of the He complexes to obtain vibrational band patterns minimally perturbed by the tag.

The spectra of the  $[M ext{ 4-CBA}]^+$   $(M = Ca^{2+} ext{ and } Mg^{2+})$ complexes are compared with that reported previously for the Ca<sup>2+</sup> propionate complex ([Ca d-OPr]<sup>+</sup>) in Figure 4. The dominant effect of complexation in the latter class of carboxylates is the dramatic collapse of the CO stretches, in that case resulting in the two bands "crossing over" such that  $\nu_{\rm as}^{\rm CO}$  falls about 30 cm<sup>-1</sup> below  $\nu_{\rm s}^{\rm CO}$ . This effect has been traced in part to the effect of the electron density being drawn onto the CO<sub>2</sub> scaffold and strengthening of the C-C bond that attaches it to the alkyl tail. At the same time, the CO2 bond angle closes by about 10° (see Table 2 for values of key structural parameters). With this trend in mind, the spectral response of the 4-CBA system to both Ca<sup>2+</sup> and Mg<sup>2+</sup> resembles that of the aliphatic system, with the dominant oscillator strength arising from the CO motions concentrated in the 1400 cm<sup>-1</sup> region. This agrees with the calculated spectra (inverted in Figure 4e,g for Ca and Mg, respectively) which correspond to the minimum energy structures displayed as insets in Figure 4d,f, respectively). These structures retain planar structure of the CBA scaffold. We note that the nominal CO stretching modes are calculated to be even more mixed with displacements of atoms on the scaffold in the 4-CBA case than those found in the aliphatic M2+ complex.5 Further

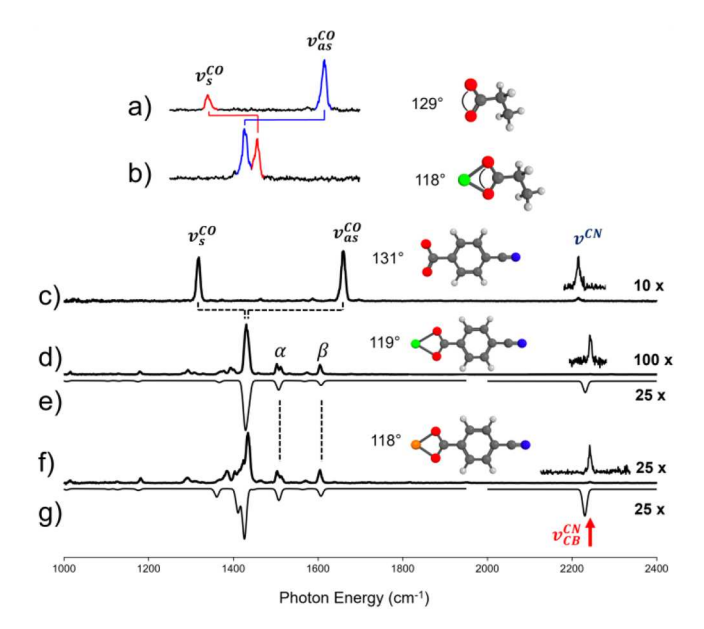


**Figure 4.** IRPD spectra of (a) H<sub>2</sub>-tagged d-OPr<sup>-</sup>, (b) He-tagged [Ca d-OPr]<sup>+</sup>, (c) D<sub>2</sub>-tagged 4-CBA<sup>-</sup>, (d) He-tagged [Ca 4-CBA]<sup>+</sup>, and (f) He-tagged [Mg 4-CBA]<sup>+</sup>. Scaled, inverted computational spectra are presented for (e) [Ca 4-CBA]<sup>+</sup> and (g) [Mg 4-CBA]<sup>+</sup>. Computational spectra are normalized to the strongest feature. The normalized *y*-axis is expanded 25 times above 2000 cm<sup>-1</sup> to make the calculated CN transitions visible. The red arrow labeled  $\nu_{\rm CB}^{\rm CN}$  marks the position of  $\nu^{\rm CN}$  in isolated benzonitrile. The bands labeled α and β in (d), (e), (f), and (g) are traced to mixed character bands involving ring CH bending displacements. See Section IIB for discussion of scaling factors. Only the fingerprint region is shown for clarity; for full spectra of the ions considered by this work, see Figure S5.

dissection of the normal mode character is beyond the scope of this paper, however, especially in light of the well-documented pitfalls that can come from overinterpreting the structural implications of the splitting between the expected  $\nu_{\rm s}^{\rm CO}$  and  $\nu_{\rm as}^{\rm CO}$  modes.  $^{30,31}$ 

Interestingly, the CN stretching fundamentals in both the Ca $^{2+}$  and Mg $^{2+}$  complexes ( $\nu^{\rm CN}$  in Figure 4d,f, respectively) occur very close to that observed for the neutral cyanobenzene molecule ( $\nu^{\rm CN}_{\rm CB}$ , red arrow in Figure 4g). This is consistent with the scenario that the partial charge delocalization from the carboxylate onto the ring in the bare [4-CBA] $^-$  does not occur to the same extent as it does in the metal complexes.The general trend that the CN stretch weakens and blue shifts from [4-CBA] $^-$  to [M 4-CBA] $^+$  is in agreement with the previously established nitrile response to the incorporation of electron withdrawing groups on the ring.  $^{25,32}$ 

Figure 5 compares the calculated potential energy curves for rotation of the carboxylate group for [4-CBA]<sup>-</sup> (red) and [Ca 4-CBA]<sup>+</sup> (green). Interestingly, the complexation with the dication substantially increases the barrier, from 3.92 to 8.70 kcal/mol (see Table 2). At a qualitative level, this large effect would appear to be correlated with the polarizability of the CBA scaffold, such that the planar structure enables substantial negative charge to be accumulated onto the carboxylate when conjugated with the ring. When this characteristic is lost in the perpendicular arrangement ( $\theta = 90^{\circ}$ ), reduced enhancement of the ion binding pocket might lead to an increase in the barrier. The CO<sub>2</sub> bond angle is calculated to increase by ~0.6° in going from the planar to the perpendicular geometries, consistent with such a scenario.

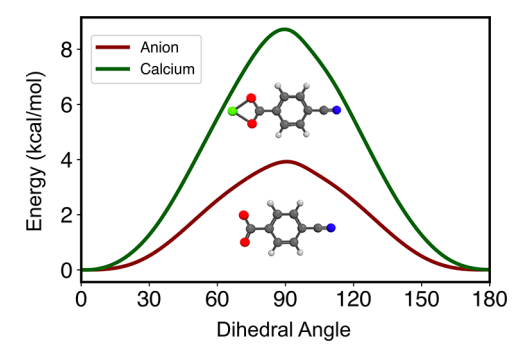


**Figure 5.** Calculated (MP2/6-311++G(d,p)) potential energy curves for rotation of the carboxylate group about the C–C bond to the ring for the [Ca 4-CBA]<sup>+</sup> cation (green) and [4-CBA]<sup>-</sup> (red). See Figure 3 and the text in Section IIB for definition of the dihedral angle and theoretical details. See Figure S6 for analogous potential energy curves obtained using DFT.

IIIB.2. M<sup>2+</sup> Complexation with 3- and 2-CBA: Emergence of the Tridentate Coordination Motif. Figure 6 presents the evolution of the vibrational spectra along the series Ca<sup>2+</sup> 4-, 3-, and 2-CBA in panels a, b, and d, respectively. The CO stretching region becomes much more cluttered in the [Ca 3-CBA]+ spectrum (Figure 6b) relative to that displayed by 4-CBA before resolving to two dominant peaks in the [Ca 2-CBA]<sup>+</sup> spectrum (Figure 6d). The strong triplet around 1500 cm<sup>-1</sup> is qualitatively captured by the computationally predicted spectrum for the [Ca 3-CBA]+ structure displayed inverted in Figure 6c. This retains the overall planar structure of the CBA scaffold, again with bidentate coordination of the Ca<sup>2+</sup> ion. The broadening of the oscillator strength derived from the CO stretches is interesting in the context of previous work on the dependence of the splitting on the electric field along the C-C bond axis.<sup>6</sup> In that study, adding solvent molecules around the divalent cation in the Ca2+ propionate complex dramatically increased the splitting as the first hydration shell "reaction" electric field acted to counter the field at the CO<sub>2</sub>- site arising from the proximal metal. Similar behavior of the CO stretches in the [Ca 3-CBA]<sup>+</sup> spectrum therefore suggests that the closer CN group is acting to slightly loosen the metal ion binding to the carboxylate. Interestingly, the CN stretch, predicted to occur at 2246 cm<sup>-1</sup>, is completely missing in the experimental spectrum. This is again a situation in which the intensity of the CN fundamental is changing by orders of magnitude while its frequency is barely affected.

With the behavior of the 4- and 3-CBA complexes in mind, at first glance it might appear that the evolution of the bands in the CO stretching region in the [Ca 2-CBA]<sup>+</sup> spectrum (Figure 6d) represents a continuation of the trend in which the bands disentangle as they decouple from nearby modes to recover their  $\nu_s^{CO}$  and  $\nu_{as}^{CO}$  parentage. The most striking difference from the other two, however, is that the CN stretch appears with dramatically increased intensity (a factor of ~50) going from 4-CBA to 2-CBA, whereas it is unmeasurably weak in the 3-CBA spectrum (Figure 6b). This intensity enhancement is accompanied by a significant (25 cm<sup>-1</sup>) shift of the CN stretch below the lowest frequency in the CBA anions, and a very large (~50 cm<sup>-1</sup>) red-shift relative to the  $\nu^{CN}$  value in [Ca 4-CBA]<sup>+</sup> (see Table 1). Note that this shift is opposite to the trend expected for a CN moiety participating in an H-bond-accepting interaction in a quasilinear arrangement along the CN bond axis, which yields a blue shift.<sup>10</sup> The red shift

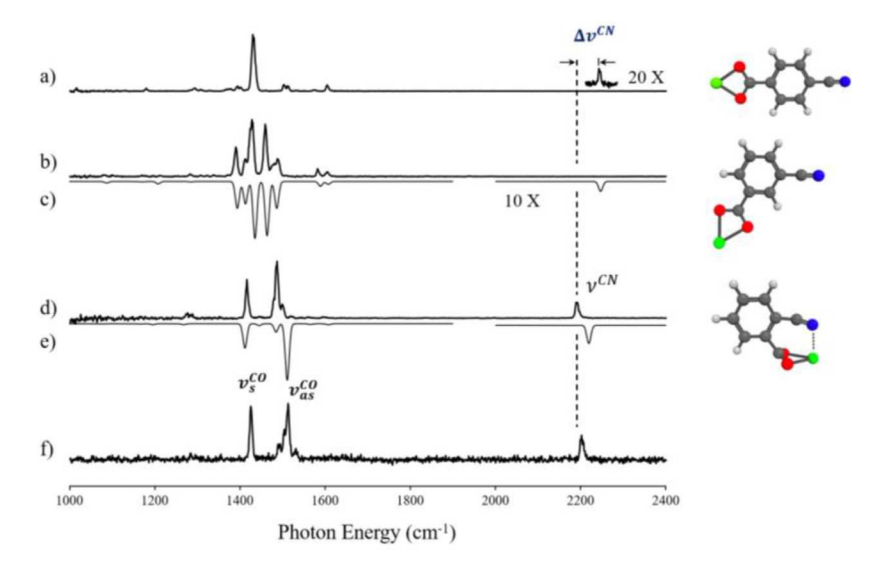
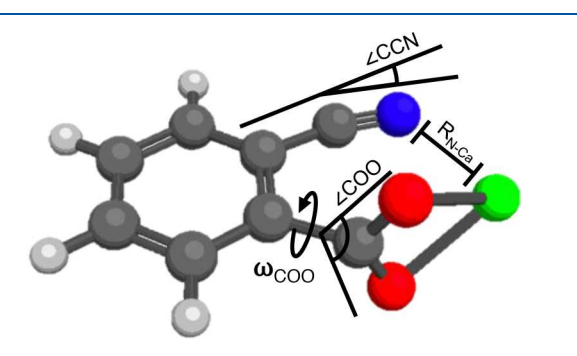


Figure 6. He-tagged IRPD spectra of CBA complexes: (a) [Ca 4-CBA]<sup>+</sup>, (b) [Ca 3-CBA]<sup>+</sup>, (d) [Ca 2-CBA]<sup>+</sup>, and (f) [Sr 2-CBA]<sup>+</sup>. Scaled, inverted computational spectra are presented for (c) [Ca 3-CBA]<sup>+</sup> and (e) [Ca 2-CBA]<sup>+</sup>. See Section IIB for mode labels and scaling factors.

observed here is, however, consistent with a side-on, or " $\pi$ ," H-bond interaction. Such H-bonding geometries have been invoked to rationalize CN line shapes in condensed media and are modeled to yield red shifts in cases where the C-N- $\delta^+$  angle is less than  $\sim 120^{\circ}$ . This is in contrast to more typical  $\sigma$  H-bonds where this angle is >120° and the usual blue shift is observed.

Both the CN frequency and intensity shifts signal the formation of a different metal ion accommodation motif that directly involves coordination with the nitrile group. The formation of a new binding configuration is confirmed by the minimum energy structure indicated in the inset of Figure 6e, where the  $-CO_2^-\cdot M^{2+}$  moiety has reoriented perpendicular to the ring, thus accommodating direct metal ion binding by the N atom of the nitrile group in an overall 3-fold coordination environment. This result also meets the structural criterion for  $\pi$  H-bonding with a C-N-Ca<sup>2+</sup> angle of 112.1° and displays a lengthened CN bond (1.181 Å) relative to [Ca 4-CBA]+ (1.178 Å) as expected in this case. The calculated spectrum for this tridentate structure indeed recovers both the behavior of the CO stretches as well as the location and intensity of the CN stretch. Key parameters for this structure are highlighted in Figure 7 and included in Table 2. To address whether this tridentate motif is a general feature of divalent metal ion



**Figure 7.** Expanded view of the tridentate structural motif adopted by the  $[Ca\ 2-CBA]^+$  complex, calculated at the MP2/6-311++G(d,p) level. The structural parameters whose values appear in Table 2 are labeled.

binding, we also recorded the spectrum of [Sr 2-CBA]<sup>+</sup> with the result presented in Figure 6f. The key spectral signatures of the tricoordinated arrangement are indeed almost identical with those displayed by the Ca<sup>2+</sup> variation, thus establishing that this mode of divalent binding is likely a common structure.

The tridentate structure adopted by [Ca 2-CBA]+ is interesting from the perspective of the intramolecular interactions at play. Specifically, we noted above that in the ortho position, the CO2 group in 2-CBA undergoes a repulsive interaction with the proximal CN group, forcing it out of plane and distorting the CN bond away from the symmetry axis of the ring. It is apparent that bringing in the Ca<sup>2+</sup> ion, with its attraction to the N atom of the nitrile group, forces the CO<sub>2</sub> further away while the cation becomes closer. This balance of attractive and repulsive interactions is manifest in the structure of the tridentate binding pocket, which now features distortion of the CN toward the net positive charge center. Note that in the perpendicular orientation of the carboxylate group in the [Ca 2-CBA]<sup>+</sup> structure (relative to the ring plane), the two CO stretches are largely decoupled from the ring modes, accounting for the simple doublet structure in the 1500 cm<sup>-1</sup> region. In the context of the local electric field model mentioned above, it appears that the presence of the CN in the first coordination shell around the Ca<sup>2+</sup> ion plays a similar role as addition of two or three water molecules in the microhydrated [Ca d-OPr]+ case.6

To further explore the competition of intramolecular interactions at play in the metal complexes with 2-CBA, we again calculated the potential energy surfaces describing rotation of the  $CO_2$  group about the C–C bond axis, with the results displayed in Figure 8. Interestingly, at a rotation angle of about  $60^{\circ}$ , there is a discontinuity in the curve associated with a change in the binding motif for the lowest energy structure, leading to a high-energy local minimum. In the binding motif of this local minimum, the  $Ca^{2+}$  binds to one of the oxygen atoms in a monodentate fashion while binding side-on to the N atom of the nitrile group to form a seven-membered ring. This local contact to the CN group is quite similar to that found in the tridentate ground state structure.

We next address the role of the charge state of the metal ion in driving these chelation motifs by extending the theoretical

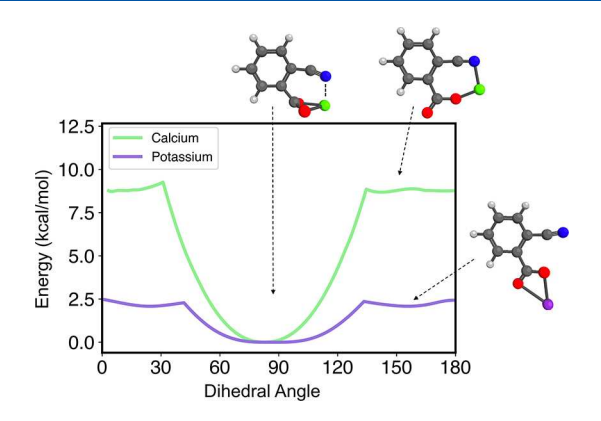


**Figure 8.** Calculated (MP2/6-311++G(d,p)) potential energy curves for rotation of the  $-CO_2^-$  group about the C–C bond to the ring when the carboxylate group is coordinated to  $Ca^{2+}$  (green) and  $K^+$  (purple). See Figure 3 and text in Section IIB for the definition of the dihedral angle and theoretical details. See Figure S7 for analogous potential energy curves obtained using DFT.

study to include the neutral  $[K\ 2\text{-CBA}]$  system, with the results presented as the purple curve in Figure 8. In that case, the minimum energy structure occurs with the  $CO_2^-\cdot K^+$  moiety oriented at  $85.57^\circ$  relative to the ring. Apparently, the singly charged ion does not provide sufficient attraction to the nitrile to fully overcome the energetic cost of completely breaking the conjugation of the  $CO_2$  group with the ring. In addition, the planar structure occurs with retention of the bidentate binding of  $K^+$  to the carboxylate, illustrating the importance of the greater electrostatic interactions at play in the  $M^{2+}$  systems.

### IV. CONCLUSIONS

We have analyzed the vibrational spectra of three cryogenically cooled anionic cyanobenzoate isomers and their positively charged complexes with Ca2+, Mg2+, and Sr2+. The anion spectra yield simple patterns dominated by the symmetric and asymmetric CO stretches of the carboxylate headgroup along with a much weaker isolated CN stretching fundamental near 2220 cm<sup>-1</sup>. The 2-CBA isomer, with the -CO<sub>2</sub> and CN groups in close proximity, adopts a nonplanar configuration in which repulsion between one of the carboxylate oxygens and the neighboring nitrile moiety distorts the ground state geometry such that these groups are deflected away from each other. The barrier to rotation of the carboxylate group is lowered by about 40% relative to that in the other isomers by this effect. Although the CN stretching frequency only changes by  $\sim 10 \text{ cm}^{-1}$  across the three anionic species, the intensity is observed to be much lower (by about a factor of 3) in the case of the strongly distorted 2-CBA isomer.

For the 3- and 4-CBA isomers, divalent metal ion attachment occurs in a bidentate fashion like that of the structures reported earlier for metal ion complexes with aliphatic carboxylates. This arrangement retains the planar structure of the 3- and 4-CBA anions and is evidenced by the collapse of the CO stretches in response to charge accumulation on the carboxylate group as well as reduction in the  $\rm CO_2$  bond angle (by about  $10^{\circ}$ ). The spectral signatures of this motif are very similar upon attachment of the  $\rm Ca^{2+}$  and  $\rm Mg^{2+}$  ions. The CN stretches in the 3- and 4-isomers are blueshifted relative to the location in the anion, falling close to the value found in neutral benzonitrile.

The behavior of the [M 2-CBA]<sup>+</sup> isomer is markedly different: the intensity of the CN stretch is dramatically

enhanced (by  $\sim 50\times$ ) and strongly red-shifted (by  $\sim 50 \text{ cm}^{-1}$ ) relative to the bands in the 3- and 4-CBA metal complexes. This occurs with a more open splitting in the CO stretching bands. These features are traced to a new structural motif in which the  $-\text{CO}_2^{-\cdot}\text{M}^{2+}$  moiety adopts a tridentate coordination environment involving attachment to both oxygen atoms as well to the N atom of the CN group. This occurs with rotation of the CO<sub>2</sub> group perpendicular to the plane of the ring. The large red shift of the CN upon this "sideways" complexation to M2+ is opposite to the usual blue shifts displayed by "Lewis acid" or  $\sigma$ -H-bond-like complexation directly along the CN bond axis and is consistent with a metal-CN interaction in a geometry resembling a  $\pi$  H-bond. Divalent metal ion complexation onto 2-CBA thus reflects two intramolecular forces: the repulsion between the oxygen atoms on the carboxylate and the proximal nitrile group and the attraction of metal ions to the nitrile group. This compromise is explored with theoretical calculations on the neutral [K 2-CBA] complex, which is calculated to occur with an intermediate structure in which the  $-CO_2^- \cdot K^+$  moiety is displaced slightly from the perpendicular arrangement adopted by the divalent

This work provides insights into the balance of electrostatic and steric interactions among metal ions, carboxylate groups, and nitrile groups, leading to a variety of structural motifs that can be probed spectroscopically and computationally. These insights have implications for a wide range of chemical and biological systems.

#### ASSOCIATED CONTENT

# **Supporting Information**

The Supporting Information is available free of charge at https://pubs.acs.org/doi/10.1021/acs.jpca.2c07658.

Comparison of anion IRPD spectra to computation, absolute potential energy curves for  $-\mathrm{CO_2}^-$  rotation in anionic species, IRPD spectra for all species considered by this work, potential energy curves for  $-\mathrm{CO_2}^-$  rotation in  $\mathrm{Mg^{2^+}}$  and  $\mathrm{Ca^{2^+}}$  complexes, Cartesian coordinates for minimum energy structures, and DFT results (PDF)

# AUTHOR INFORMATION

# **Corresponding Author**

Mark A. Johnson — Sterling Chemistry Laboratory
Department of Chemistry, Yale University, New Haven,
Connecticut 06512, United States; orcid.org/0000-00021492-6993; Email: mark.johnson@yale.edu

#### **Authors**

Ahmed Mohamed – Sterling Chemistry Laboratory Department of Chemistry, Yale University, New Haven, Connecticut 06512, United States

Sean C. Edington — Sterling Chemistry Laboratory
Department of Chemistry, Yale University, New Haven,
Connecticut 06512, United States; orcid.org/0000-00025894-8801

Maxim Secor — Sterling Chemistry Laboratory Department of Chemistry, Yale University, New Haven, Connecticut 06512, United States; orcid.org/0000-0003-2569-2384

James R. Breton – Sterling Chemistry Laboratory Department of Chemistry, Yale University, New Haven, Connecticut 06512, United States; orcid.org/0000-0002-0410-1285 Sharon Hammes-Schiffer — Sterling Chemistry Laboratory Department of Chemistry, Yale University, New Haven, Connecticut 06512, United States; orcid.org/0000-0002-3782-6995

Complete contact information is available at: https://pubs.acs.org/10.1021/acs.jpca.2c07658

# **Author Contributions**

\*A.M. and S.C.E. contributed equally to this work.

#### Notes

The authors declare no competing financial interest.

#### ACKNOWLEDGMENTS

M.A.J. thanks the NSF under grant CHE-1900119 for support of our effort to elucidate spectral markers for divalent metal ion binding onto polyoxyanions and AFOSR for support under the MURI grant 62742085-204669 for our work on the molecular mechanism of CN electric field reporters. We thank Payten Harville for assistance in acquiring the data for the [Sr 2-CBA] + complex. A.M. thanks the National Institutes of Health for support through the Predoctoral Program in Biophysics T32 GM008283. Research reported in this publication was also supported by the National Institute of General Medical Sciences of the National Institutes of Health under award number 5T32GM067543-20. 10% of this project's costs were financed with this NIH support, and 100% of this project's costs were financed with federal funds including NIH support. 0% of this project's costs were financed by nongovernmental sources. S.H.-S. acknowledges support from the Air Force Office of Scientific Research (AFOSR) under AFOSR Award No. FA9550-18-1-0420 for studying theoretical aspects of CN reporters and the Center for Molecular Electrocatalysis, an Energy Frontier Research Center funded by the U.S. Department of Energy, Office of Science, Basic Energy Sciences for supporting M.S. The content is solely the responsibility of the authors and does not necessarily represent the official views of the National Institutes of Health. Special thanks to Dr. Michael Berman. His insight and encouragement led to breakthrough instrumental advances in cryogenic ion chemistry and spectroscopy that not only made possible the measurements reported here but also opened the way for ion spectroscopy to play a meaningful role in the design and optimization of contemporary chemical processes. His support and encouragement have also been vital to the theoretical chemistry community.

# REFERENCES

- (1) Dudev, T.; Lim, C. Monodentate Versus Bidentate Carboxylate Binding in Magnesium and Calcium Proteins: What Are the Basic Principles? *J. Phys. Chem. B* **2004**, *108* (14), 4546–4557.
- (2) Dudev, T.; Lim, C. Effect of Carboxylate-Binding Mode on Metal Binding/Selectivity and Function in Proteins. *Acc. Chem. Res.* **2007**, 40 (1), 85–93.
- (3) Nara, M.; Tanokura, M. Infrared Spectroscopic Study of the Metal-Coordination Structures of Calcium-Binding Proteins. *Biochem. Biophys. Res. Commun.* **2008**, 369 (1), 225–239.
- (4) Edington, S. C.; Gonzalez, A.; Middendorf, T. R.; Halling, D. B.; Aldrich, R. W.; Baiz, C. R. Coordination to Lanthanide Ions Distorts Binding Site Conformation in Calmodulin. *Proc. Natl. Acad. Sci. U. S. A.* 2018, 115 (14), E3126–E3134.
- (5) DePalma, J. W.; Kelleher, P. J.; Tavares, L. C.; Johnson, M. A. Coordination-Dependent Spectroscopic Signatures of Divalent Metal Ion Binding to Carboxylate Head Groups: H<sub>2</sub>- and He-Tagged

- Vibrational Spectra of  $M^{2+}$ ·RCO<sub>2</sub><sup>-</sup> (M = Mg and Ca, R = -CD<sub>3</sub>, -CD<sub>2</sub>CD<sub>3</sub>) Complexes. *J. Phys. Chem. Lett.* **2017**, 8 (2), 484–488.
- (6) Denton, J. K.; Kelleher, P. J.; Johnson, M. A.; Baer, M. D.; Kathmann, S. M.; Mundy, C. J.; Wellen Rudd, B. A.; Allen, H. C.; Choi, T.; Jordan, K. D. Molecular-Level Origin of the Carboxylate Head Group Response to Divalent Metal Ion Complexation at the Air-Water Interface. *Proc. Natl. Acad. Sci. U. S. A.* **2019**, *116* (30), 14874—14880.
- (7) Fried, S. D.; Boxer, S. G. Electric Fields and Enzyme Catalysis. *Annu. Rev. Biochem.* **2017**, *86* (1), 387–415.
- (8) Baiz, C. R.; Błasiak, B.; Bredenbeck, J.; Cho, M.; Choi, J.-H.; Corcelli, S. A.; Dijkstra, A. G.; Feng, C.-J.; Garrett-Roe, S.; Ge, N.-H.; et al. Vibrational Spectroscopic Map, Vibrational Spectroscopy, and Intermolecular Interaction. *Chem. Rev.* **2020**, *120* (15), 7152–7218.
- (9) Weaver, J. B.; Kozuch, J.; Kirsh, J. M.; Boxer, S. G. Nitrile Infrared Intensities Characterize Electric Fields and Hydrogen Bonding in Protic, Aprotic, and Protein Environments. *J. Am. Chem. Soc.* **2022**, *144* (17), 7562–7567.
- (10) Slocum, J. D.; Webb, L. J. Measuring Electric Fields in Biological Matter Using the Vibrational Stark Effect of Nitrile Probes. *Annu. Rev. Phys. Chem.* **2018**, *69* (1), 253–271.
- (11) First, J. T.; Slocum, J. D.; Webb, L. J. Quantifying the Effects of Hydrogen Bonding on Nitrile Frequencies in GFP: Beyond Solvent Exposure. *J. Phys. Chem. B* **2018**, 122 (26), 6733–6743.
- (12) Layfield, J. P.; Hammes-Schiffer, S. Calculation of Vibrational Shifts of Nitrile Probes in the Active Site of Ketosteroid Isomerase Upon Ligand Binding. *J. Am. Chem. Soc.* **2013**, *135* (2), 717–725.
- (13) Choi, J.-H.; Oh, K.-I.; Lee, H.; Lee, C.; Cho, M. Nitrile and Thiocyanate IR Probes: Quantum Chemistry Calculation Studies and Multivariate Least-Square Fitting Analysis. *J. Chem. Phys.* **2008**, *128* (13), 134506.
- (14) Oh, K.-I.; Choi, J.-H.; Lee, J.-H.; Han, J.-B.; Lee, H.; Cho, M. Nitrile and Thiocyanate IR Probes: Molecular Dynamics Simulation Studies. *J. Chem. Phys.* **2008**, *128* (15), 154504.
- (15) Menges, F. S.; Perez, E. H.; Edington, S. C.; Duong, C. H.; Yang, N.; Johnson, M. A. Integration of High-Resolution Mass Spectrometry with Cryogenic Ion Vibrational Spectroscopy. *J. Am. Soc. Mass Spectrom.* **2019**, *30* (9), 1551–1557.
- (16) Head-Gordon, M.; Pople, J. A.; Frisch, M. J. MP2 Energy Evaluation by Direct Methods. *Chem. Phys. Lett.* **1988**, *153* (6), 503–506.
- (17) Frisch, M. J.; Head-Gordon, M.; Pople, J. A. A Direct MP2 Gradient-Method. *Chem. Phys. Lett.* **1990**, *166* (3), 275–280.
- (18) Head-Gordon, M.; Head-Gordon, T. Analytic MP2 Frequencies without 5th-Order Storage Theory and Application to Bifurcated Hydrogen-Bonds in the Water Hexamer. *Chem. Phys. Lett.* **1994**, 220 (1–2), 122–128.
- (19) Blaudeau, J.-P.; McGrath, M. P.; Curtiss, L. A.; Radom, L. Extension of Gaussian-2 (G2) Theory to Molecules Containing Third-Row Atoms K and Ca. *J. Chem. Phys.* **1997**, 107, 5016–5021.
- (20) Krishnan, R.; Binkley, J. S.; Seeger, R.; Pople, J. A. Self-Consistent Molecular Orbital Methods. XX. A Basis Set for Correlated Wave Functions. *J. Chem. Phys.* **1980**, 72 (1), 650–654.
- (21) Dunning, T. H.; Hay, P. J. Gaussian Basis Sets for Molecular Calculations. In *Methods of Electronic Structure Theory*; Schaefer, H. F., Ed.; Springer US: Boston, MA, 1977; pp 1–27.
- (22) Wachters, A. J. H. Gaussian Basis Set for Molecular Wavefunctions Containing Third-Row Atoms. *J. Chem. Phys.* **1970**, 52 (3), 1033–1036.
- (23) Frisch, M. J.; Trucks, G. W.; Schlegel, H. B.; Scuseria, G. E.; Robb, M. A.; Cheeseman, J. R.; Scalmani, G.; Barone, V.; Petersson, G. A.; Nakatsuji, H.; et al. *Gaussian 16*, Rev. B.01; Gaussian, Inc.: Wallingford, CT, 2016.
- (24) Sutton, C. C. R.; da Silva, G.; Franks, G. V. Modeling the IR Spectra of Aqueous Metal Carboxylate Complexes: Correlation between Bonding Geometry and Stretching Mode Wavenumber Shifts. *Chem.—Eur. J.* **2015**, *21* (18), 6801–6805.

- (25) Green, J. H. S.; Harrison, D. J. Vibrational Spectra of Benzene Derivatives—XVII. Benzonitrile and Substituted Benzonitriles. Spectrochim. Acta A: Mol. Spectrosc. 1976, 32 (6), 1279–1286.
- (26) Acharyya, A.; Mukherjee, D.; Gai, F. Assessing the Effect of Hofmeister Anions on the Hydrogen-Bonding Strength of Water Via Nitrile Stretching Frequency Shift. *J. Phys. Chem. B* **2020**, *124* (52), 11783–11792.
- (27) Drexler, C. I.; Cracchiolo, O. M.; Myers, R. L.; Okur, H. I.; Serrano, A. L.; Corcelli, S. A.; Cremer, P. S. Local Electric Fields in Aqueous Electrolytes. *J.Phys. Chem. B* **2021**, *125* (30), 8484–8493.
- (28) Lindquist, B. A.; Furse, K. E.; Corcelli, S. A. Nitrile Groups as Vibrational Probes of Biomolecular Structure and Dynamics: An Overview. *Phys. Chem. Chem. Phys.* **2009**, *11* (37), 8119–8132.
- (29) Zhao, R.; Shirley, J. C.; Lee, E.; Grofe, A.; Li, H.; Baiz, C. R.; Gao, J. Origin of Thiocyanate Spectral Shifts in Water and Organic Solvents. *J. Chem. Phys.* **2022**, *156* (10), 104106.
- (30) Deacon, G. B.; Phillips, R. J. Relationships between the Carbon-Oxygen Stretching Frequencies of Carboxylato Complexes and the Type of Carboxylate Coordination. *Coord. Chem. Rev.* **1980**, 33 (3), 227–250.
- (31) Deacon, G. B.; Huber, F.; Phillips, R. J. Diagnosis of the Nature of Carboxylate Coordination from the Direction of Shifts of Carbon Oxygen Stretching Frequencies. *Inorg. Chim. Acta* **1985**, *104* (1), 41–45.
- (32) Choi, S.; Park, J.; Kwak, K.; Cho, M. Substituent Effects on the Vibrational Properties of the Cn Stretch Mode of Aromatic Nitriles: IR Probes Useful for Time-Resolved IR Spectroscopy. *Chem.—Asian J.* **2021**, *16* (18), 2626–2632.

# ☐ Recommended by ACS

Unraveling the Vibrational Spectral Signatures of a Dislocated H Atom in Model Proton-Coupled Electron Transfer Dyad Systems

Liangyi Chen, Joseph A. Fournier, et al.

APRIL 07, 2023

THE JOURNAL OF PHYSICAL CHEMISTRY A

READ 🗹

Observation of Slow Eigen-Zundel Interconversion in  $H^+(H_2O)_6$  Clusters upon Isomer-Selective Vibrational Excitation and Buffer Gas Cooling in a Cryogenic Ion Trap

Thien Khuu, Mark A. Johnson, et al.

MARCH 27, 2023

JOURNAL OF THE AMERICAN SOCIETY FOR MASS SPECTROMETRY

READ 🗹

Relativistic Effects in the Ligation of Atomic Coinage Metal Cations with  $O_2$  and  $C_6H_6$ : Anomalous Formation of Relativistic Mono- and Bis-adducts with  $Au^+$ 

Voislav Blagojevic, Diethard K. Bohme, et al.

MAY 09 2022

JOURNAL OF THE AMERICAN SOCIETY FOR MASS SPECTROMETRY

READ 🗹

Gas-Phase Reactivity of Ozone with Lanthanide Ions (Sm+, Nd+) and Their Higher Oxides

Brendan C. Sweeny, Shaun G. Ard, et al.

MAY 11, 2022

JOURNAL OF THE AMERICAN SOCIETY FOR MASS SPECTROMETRY

READ 🗹

Get More Suggestions >